Hindawi Publishing Corporation
Journal of Nanomaterials
Volume 2014, Article ID 175924, 6 pages
http://dx.doi.org/10.1155/2014/175924

Research Article

Hydrothermal Synthesis of Boron-Doped MnO_2 and Its Decolorization Performance

Ming Sun, Ting Lin, Gao Cheng, Fei Ye, and Lin Yu

School of Chemical Engineering and Light Industry, Guangdong University of Technology, Guangzhou 510006, China

Correspondence should be addressed to Ming Sun; sunmgz@gmail.com

Received 18 June 2014; Revised 17 September 2014; Accepted 1 October 2014; Published 14 October 2014

Academic Editor: Young-Kuk Kim

To functionalize MnO_2 with foreign ions is one of the commonly used methods to improve the adsorption/oxidation properties of MnO_2. Boron-doped MnO_2 was prepared by the reaction of $MnSO_4$, $KMnO_4$, and boric acid by a facile hydrothermal method. Boron-MnO_2 was characterized by X-ray diffraction (XRD), Raman spectra, scanning electron microscopy (SEM), energy dispersive X-ray analysis (EDX), transmission electron microscopy (TEM), high-resolution TEM (HRTEM), selected area electron diffraction pattern (SAED), and X-ray photo-electron spectroscopy (XPS) techniques. The characterization of XPS and EDX confirms that boron has been doped into MnO_2, but the boron dopant has no obvious effect on the crystallization of MnO_2 as shown by the results of XRD and Raman characterization. The boron-doped MnO_2 nanorods display high performance in the methyl orange degradation with a decolorization degree of 90% in 2 min (5% B-MnO_2 dosage, 5 mg; methyl orange concentration, 20 mg L^{-1}).

1. Introduction

Manganese oxides have diverse structures with many derivative compounds [1]. Generally, the valence of Mn in manganese oxides can be +2, +3 or +4, and there may be two or three kinds of valence coexisting in the same crystalline structure. The characteristics in structure make manganese oxides possess unique chemical and physical properties. Thus, research on manganese oxides has received considerable attention in various fields like energy storage/conversion material [2, 3], catalysis material [4], ion-exchange material, and so forth [5]. Of all the applications, the elimination of organic pollutants or heavy metal in water has always been the focus of research from the aspect of environment protection. Manganese oxides are widely used to remove/oxide heavy metal [6, 7], acetaminophen [8], phenol [9], nonylphenol [10], naproxen [11], ciprofloxacin [12], Congo red [13], rhodamine B [14], and so forth.

The adsorption/oxidation properties of manganese oxides are generally influenced by their microstructure, shape, size, and/or composition. Therefore, long-term attention has been paid to the preparation and modification of MnO_2. Generally, there are two ways to improve the adsorption/oxidation properties of MnO_2. One way is to fabricate large-surface-area/mesoporous MnO_2 [15] or loaded MnO_2 with a high-surface-area carrier [16–18], and the other is to functionalize MnO_2 with foreign ions [19, 20]. Compared with the commonly used metal ions, nonmetal elements for MnO_2 are rarely reported [21, 22]. It is notable that nonmetal elements such as B, N, or S have been widely used as dopants for TiO_2 and proved to be very effective for enhancing the photoactivity [23]. The structure of TiO_2 and MnO_2 has somewhat similarity. Inspired by such fact, we tried to synthesis boron-doped MnO_2 via reactions among $MnSO_4$, $KMnO_4$, and boric acid under hydrothermal conditions. During the review process of our paper, very recently, Chi et al. [24] reported that boron-doped manganese dioxide showed superior electrochemical performance as supercapacitors and the boron dopant was an effective way to improve and modify the characteristics of manganese oxide. Herein, we systematically characterized the physicochemical properties of the prepared manganese oxide using various techniques. The application in the decolorization of industrial acid dye, methyl orange, was studied as probe reaction to evaluate its activity.

2. Experimental

A group of boron-doped MnO_2 were prepared by mixing $MnSO_4$ (22.1 mmol), $KMnO_4$ (16.8 mmol), and different amounts of boric acid with 55 mL H_2O under hydrothermal conditions maintained at 160°C for 24 h. The solid precipitate was collected and washed by centrifugation and then dried at 60°C. The products are marked as x% B-MnO_2, where x means the theoretical molar ratio of boron to Mn in the raw materials.

X-ray powder diffraction (XRD) was carried out using ULTIMA-III X-ray diffractometer (40 kV, 40 mA, Cu Kα radiation). Scanning electron microscopy and energy dispersive X-ray analysis (SEM-EDX) were performed on a Digital Scanning Microscope S-3400N operated at 15 kV. The transmission electron microscopy (TEM) image, selected area electron diffraction pattern (SAED) and high-resolution transmission electron microscopy (HRTEM) image were obtained on a JEOL JEM-2100HR using an acceleration voltage of 200 kV. Raman spectroscopy was recorded on a dispersive Horiva Jobin Yvon LabRam HR800 Microscope, with a 24 mW He-Ne green laser (633 nm). X-ray photoelectron spectroscopy (XPS) was obtained by a Thermo ESCALAB 250 instrument equipped with a monochromatic Al Kα (1486.6 eV) X-ray source. N_2 adsorption-desorption isotherms were measured using a Micromeritics ASAP 2020 Analyzer.

The decolorization experiment was performed in a round bottom flask at room temperature. B-MnO_2 of 5 mg was added into a solution of methyl orange (20 mg L^{-1}, 100 mL) with a pH of 1.7 adjusted by diluted H_2SO_4. A small quantity of mixture was withdrawn at definite intervals and then centrifuged to remove the sedimentation before UV analysis. The decolorization performance was calculated by UV-visible spectrum (T-245, Shimadzu) by monitoring its characteristic peak at 507 nm.

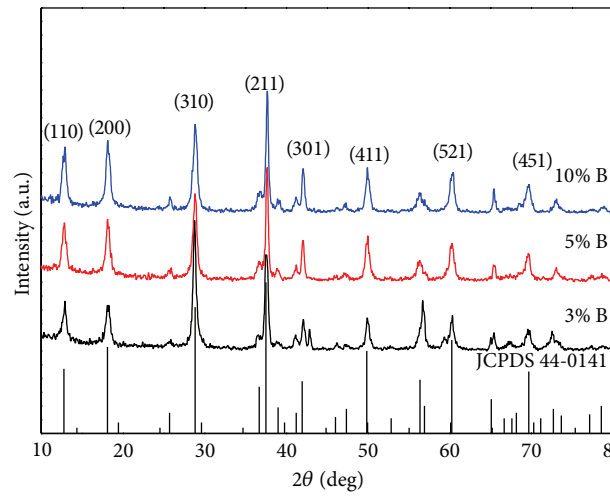

Figure 1: XRD patterns of x% B-MnO_2.

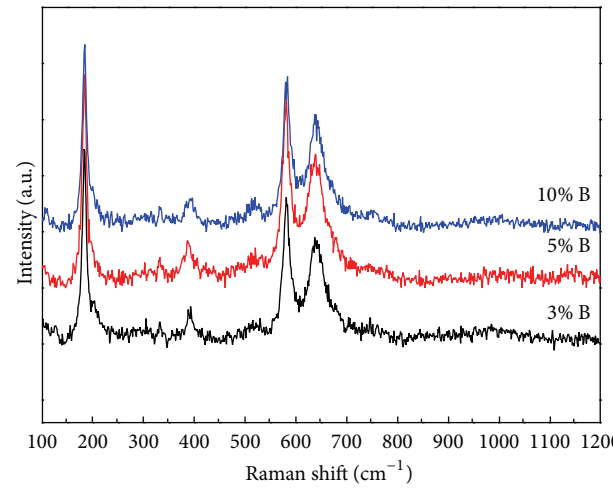

Figure 2: Raman spectra of x% B-MnO_2.

3. Results and Discussion

The structure of the B-doped MnO_2 was characterized by XRD and Raman spectroscopy as displayed in Figures 1 and 2, respectively. Figure 1 shows the XRD patterns with peaks located at $2\theta = 12.6°, 17.8°, 28.5°, 37.3°, 41.8°, 49.7°$, and $60.0°$, which match well with the standard patterns of α-MnO_2 (JCPDS 44-0141). With boron dopant increasing, no vital difference for the XRD peaks is observed. Besides, the peaks belonging to borate impurities are not detected.

The Raman spectra (Figure 2) are almost identical for all the samples, indicating that the amount of boron dopant had no effect on the structure of MnO_2. The Raman spectra feature four main bands at 187, 392, 582, and 647 cm^{-1}. The two Raman bands at 582 and 647 cm^{-1} are indicative of the vibration modes of MnO_6 octahedron [25]. No peaks at around 770 cm^{-1} and 805 cm^{-1}, corresponding to $[BO_4]$ tetrahedron and B_2O_3, are found [26], and this observation proves that no isolate boron exists.

Figure 3 shows one-dimensional stacked rod-like morphologies of B-MnO_2 with the length of hundreds of nanometers, and this result is in agreement with that observed by Ma et al. [13]. No vital difference can be found with the rise of boron doping. The TEM image in Figure 4(a) clearly shows 5% B-MnO_2 is in a typical nanorod shape with various lengths and a diameter of about 35 nm. The representative HRTEM is given in Figure 4(b). The separated spacing of 0.49 nm corresponds to (200) plane in the α-MnO_2 crystal structure. The single crystal feature of B-MnO_2 is proved by the inset electron diffraction image, which shows the B-MnO_2 nanorod grows along the [001] crystal direction. The SAED pattern also confirms the single crystal feature of the B-MnO_2. The TEM and HRTEM results are consistent with the XRD and Raman data, verifying the good crystallinity of the B-MnO_2. Elementary composition analysis by EDX and XPS confirms the presence of boron (Figures 4(c) and 4(d)). The EDX spectrum demonstrates peaks of O, K, Mn, and B. The binding energy located at around 198 eV for B 1s is different from the B 1s of H_3BO_3 or B_2O_3 located at 192~193 eV [27].

Figure 5 shows the nitrogen adsorption-desorption isotherms. The B-MnO_2 nanorod possesses a typical type II

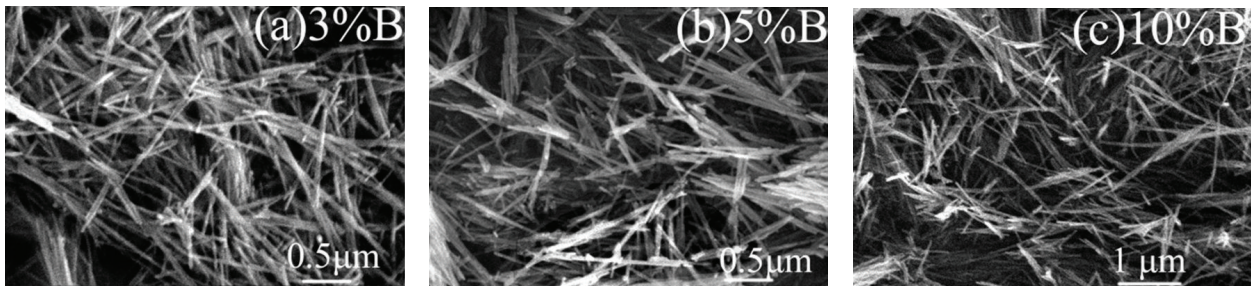

(a) (b) (c)

Figure 3: SEM images of x% B-MnO_2.

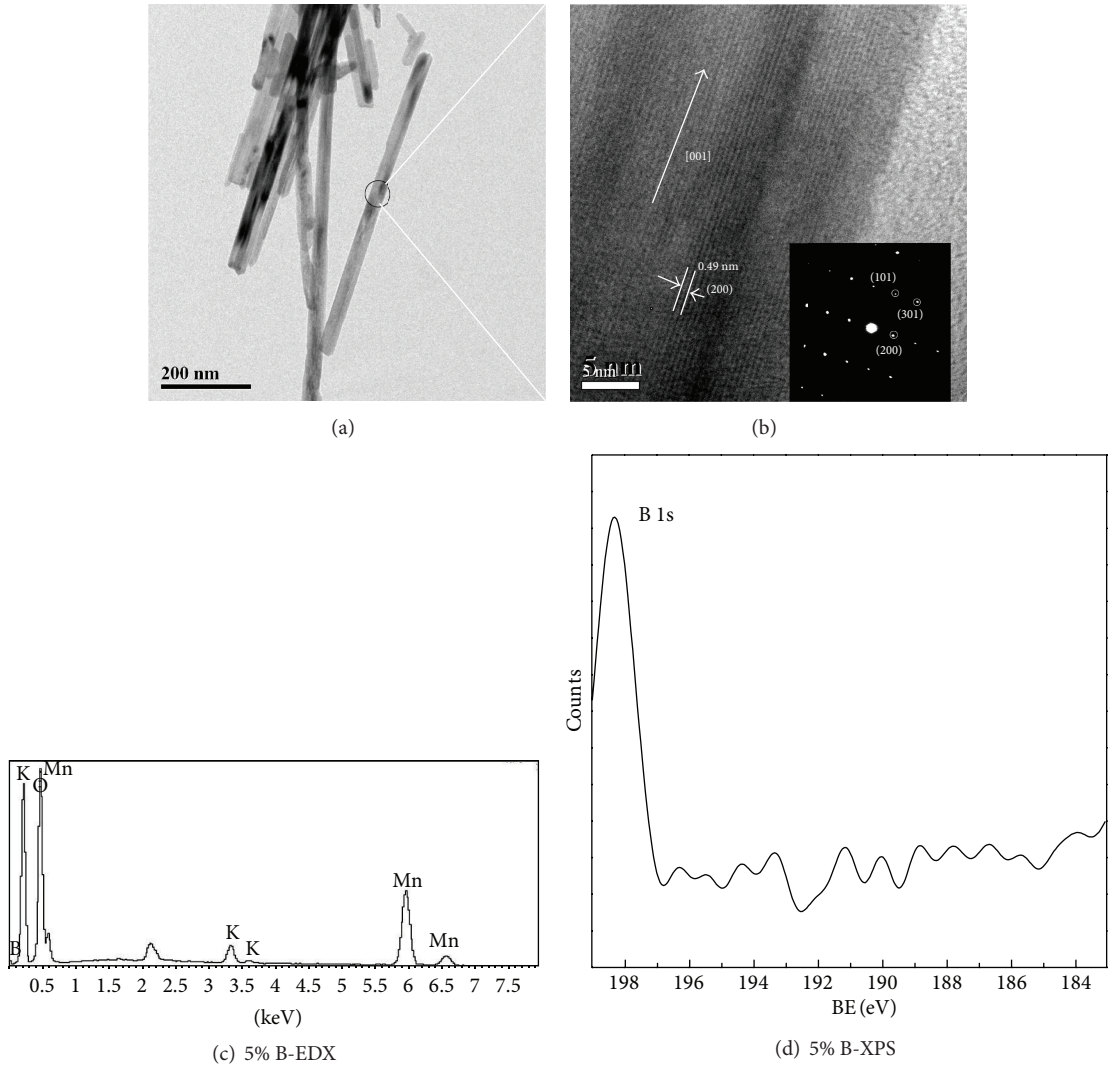

(a) (b)

(c) 5% B-EDX (d) 5% B-XPS

Figure 4: TEM and HRTEM image, EDX, and XPS of 5% B-MnO_2 sample.

isotherm with an H3-type hysteresis loop, which is indicative of slit-like pores. The BET surface area of the B-MnO_2 materials is also listed in the figure, ranging from 37 to 54 m^2/g.

Methyl orange (MO) decolorization is selected to study the decomposition properties of B-MnO_2 (Figure 6). The degree of decolorization is expressed as $(A_0 - A)/A_0$, where A_0 is the initial absorption of peak wavelength (507 nm) and A is the absorption after decolorization in different reaction time. Blank test is done in a solution of methyl orange (20 mg L^{-1}, 100 mL) without B-MnO_2, and no color change is observed at room temperature. The B-MnO_2

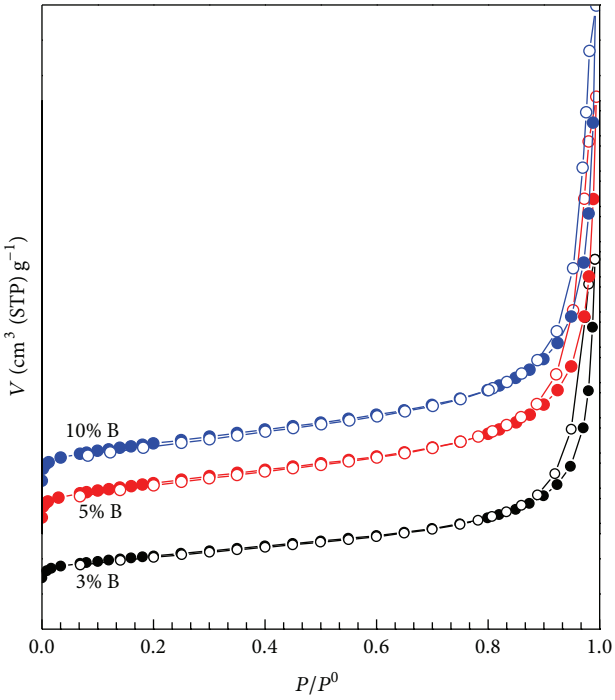

Figure 5: Nitrogen adsorption/desorption isotherms of x% B-MnO_2 nanorods.

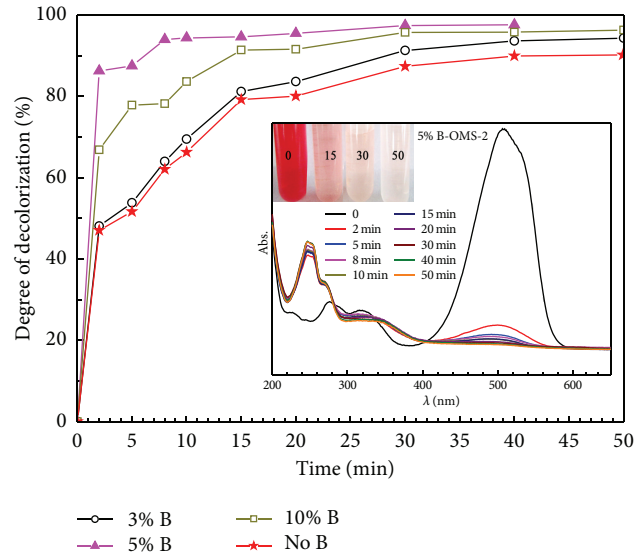

Figure 6: Decolorization performance of x% B-MnO_2 for methyl orange.

nanorods show remarkable decolorization performance for MO, and the decolorization degree reaches 97% in 50 min. The ability of the nanostructured B-MnO_2 follows the order as 5% B > 10% B > 3% B > 0% B. The activity order shows that (1) the boron dopant on MnO_2 can enhance the activity and that (2) the amount of boron dopant has optimum value. Compared with the 3% B sample, the 5% B and 10% B samples have relatively larger surface area, which will benefit the MO degradation; thus they have relatively good performance. We tentatively deduced that too much boron present on the 15% B-MnO_2 sample and excessive boron may block the tunnel of the MnO_2, which will hamper its activity. The inset figure (Figure 6) displays the UV-Vis absorption spectra of MO under the reaction with 5% B-MnO_2. The characteristic absorption peak at 507 nm decreases sharply with prolonged time. Within 2 min, the value of peak is reduced at least an order of magnitude, and the decolorization degree reaches nearly 90%. After 50 min, the color of the solution changes from bright red to colorless.

Usually, as an acid dye, the MO contained in wastewater is discharged under acid conditions; this is why we perform the experiment under acid conditions. Under pH lower than the isoelectric point (4.7) [28], the surface of MnO_2 is positively charged by protonation, and the electrostatic attraction between the surface and the anion group ($R\text{-}SO_3^-$) of MO contributes a lot to the absorption. This is also true in our case for B-MnO_2 with an isoelectric point of about 2.0. It is interesting that even when the concentration of MO is increased from 20 mg L^{-1} to 40 mg L^{-1} the used B-MnO_2 is still capable of decolorizing MO efficiently. As for such a high concentration of MO, apparently, pure adsorption is not enough to explain the decolorizing ability. Kuan and Chan [28] pointed out that methyl blue could be adsorbed or oxidized by tunneled manganese oxide. Similarly, MO can also be oxidized by B-MnO_2. Figure 5 shows that a new peak at around 250 nm appeared after 2 min, inferring an intermediate produced by the oxidation of MO. The oxidation ability may come from the excess surface oxygen of B-MnO_2 [19, 28]. Based on the above analysis, we can say that both adsorption and oxidation degradation play a role in the decolorizing of MO. Zhang et al. [29] also reported that the mechanism for decoloration of methyl blue can be attributed to oxidation degradation as well as adsorption. However, one thing to point out is that, under the acid conditions, the B-MnO_2 can dissolve slowly into the solvent. After the decolorization test over 5% B-MnO_2, we have detected about 20 ppm Mn^{2+} using atomic absorption spectrometry.

Hydrogen peroxide or *tert*-butyl hydroperoxide was used in some reported decolorization reactions [14, 19, 30]. However, in this study, the addition of H_2O_2 caused large amount of gas bubble, and the color of the solution did not change at all after 50 min. This is because MnO_2 is consumed preferentially by the decomposition of H_2O_2, thus leading to the failure of decolorization. Therefore, H_2O_2 is not necessary in our case.

4. Conclusions

In summary, different amounts of boron-doped α-MnO_2 nanostructures have been prepared by hydrothermal route. The dopant boron has no effect on the structure of MnO_2. The B-MnO_2 showed nanorods morphology with length of few

hundred nanometers. The 5% B-MnO_2 exhibited the highest efficiency in the MO decolorization without the assistance of H_2O_2. The prepared B-MnO_2 is promising to be used in degradation of other organic pollutants.

Conflict of Interests

The authors declare that there is no conflict of interests regarding the publication of this paper.

Acknowledgments

This work was supported by the National Natural Science Foundation of China (21306026), Natural Science Foundation of Guangdong (S2012010009680), Foundation of Higher Education of Guangdong Province (cgzhzd1104, 2013-CXZDA016), and Foundation for Distinguished Young Talents in Higher Education of Guangdong (2013LYM0024).

References

[1] Z. Chen, Z. Jiao, D. Pan et al., "Recent advances in manganese oxide nanocrystals: fabrication, characterization, and microstructure," *Chemical Reviews*, vol. 112, no. 7, pp. 3833–3855, 2012.

[2] S.-H. Li, Q.-H. Liu, L. Qi, L.-H. Lu, and H.-Y. Wang, "Progress in research on manganese dioxide electrode materials for electrochemical capacitors," *Chinese Journal of Analytical Chemistry*, vol. 40, no. 3, pp. 339–346, 2012.

[3] X. Liu, C. Chen, Y. Zhao, and B. Jia, "A review on the synthesis of manganese oxide nanomaterials and their applications on lithium-ion batteries," *Journal of Nanomaterials*, vol. 2013, Article ID 736375, 7 pages, 2013.

[4] J. Shan, Y. Zhu, S. Zhang, T. Zhu, S. Rouvimov, and F. Tao, "Catalytic performance and in situ surface chemistry of pure α-MnO_2 nanorods in selective reduction of NO and N_2O with CO," *The Journal of Physical Chemistry C*, vol. 117, no. 16, pp. 8329–8335, 2013.

[5] C.-H. Chen and S. L. Suib, "Control of catalytic activity via porosity, chemical composition, and morphology of nanostructured porous manganese oxide materials," *Journal of the Chinese Chemical Society*, vol. 59, no. 4, pp. 465–472, 2012.

[6] T. Zhang and D. D. Sun, "Removal of arsenic from water using multifunctional micro-/nano-structured MnO_2 spheres and microfiltration," *Chemical Engineering Journal*, vol. 225, pp. 271–279, 2013.

[7] M. Hua, S. Zhang, B. Pan, W. Zhang, L. Lv, and Q. Zhang, "Heavy metal removal from water/wastewater by nanosized metal oxides: a review," *Journal of Hazardous Materials*, vol. 211-212, pp. 317–331, 2012.

[8] H. Xiao, H. Song, H. Xie, W. Huang, J. Tan, and J. Wu, "Transformation of acetaminophen using manganese dioxide-mediated oxidative processes: reaction rates and pathways," *Journal of Hazardous Materials*, vol. 250-251, pp. 138–146, 2013.

[9] E. Saputra, S. Muhammad, H. Sun, H.-M. Ang, M. O. Tadé, and S. Wang, "Manganese oxides at different oxidation states for heterogeneous activation of peroxymonosulfate for phenol degradation in aqueous solutions," *Applied Catalysis B: Environmental*, vol. 142-143, pp. 729–735, 2013.

[10] Z. Lu and J. Gan, "Oxidation of nonylphenol and octylphenol by manganese dioxide: kinetics and pathways," *Environmental Pollution*, vol. 180, pp. 214–220, 2013.

[11] Y. Zhang, Y. Yang, T. Zhang, and M. Ye, "Heterogeneous oxidation of naproxen in the presence of α-MnO_2 nanostructures with different morphologies," *Applied Catalysis B: Environmental*, vol. 127, pp. 182–189, 2012.

[12] X. Xiao, S.-P. Sun, M. B. McBride, and A. T. Lemley, "Degradation of ciprofloxacin by cryptomelane-type manganese(III/IV) oxides," *Environmental Science and Pollution Research*, vol. 20, no. 1, pp. 10–21, 2013.

[13] H. Ma, J. Shen, M. Shi, B. Yan, N. Li, and M. Ye, "Facile and template-free preparation of α-MnO_2 nanostructures and their enhanced adsorbability," *Materials Research Bulletin*, vol. 46, no. 9, pp. 1461–1466, 2011.

[14] N. Sui, Y. Duan, X. Jiao, and D. Chen, "Large-scale preparation and catalytic properties of one-dimensional α/β-MnO_2 nanostructures," *Journal of Physical Chemistry C*, vol. 113, no. 20, pp. 8560–8565, 2009.

[15] S. Sun, W. Wang, M. Shang, J. Ren, and L. Zhang, "Efficient catalytic oxidation of tetraethylated rhodamine over ordered mesoporous manganese oxide," *Journal of Molecular Catalysis A: Chemical*, vol. 320, no. 1-2, pp. 72–78, 2010.

[16] J. Wang, L. Liu, L. Han, Y. Hu, L. Chang, and W. Bao, "Alumina-supported manganese oxide sorbent prepared by sub-critical water impregnation for hot coal gas desulfurization," *Fuel Processing Technology*, vol. 110, pp. 235–241, 2013.

[17] C. Luo, R. Wei, D. Guo, S. Zhang, and S. Yan, "Adsorption behavior of MnO_2 functionalized multi-walled carbon nanotubes for the removal of cadmium from aqueous solutions," *Chemical Engineering Journal*, vol. 225, pp. 406–415, 2013.

[18] Y. Li, Q. Du, J. Wang et al., "Defluoridation from aqueous solution by manganese oxide coated graphene oxide," *Journal of Fluorine Chemistry*, vol. 148, pp. 67–73, 2013.

[19] T. Sriskandakumar, N. Opembe, C.-H. Chen, A. Morey, C. King'Ondu, and S. L. Suib, "Green decomposition of organic dyes using octahedral molecular sieve manganese oxide catalysts," *The Journal of Physical Chemistry A*, vol. 113, no. 8, pp. 1523–1530, 2009.

[20] R. Jothiramalingam, T. M. Tsao, and M. K. Wang, "High-power ultrasonic-assisted phenol and dye degradation on porous manganese oxide doped titanium dioxide catalysts," *Kinetics and Catalysis*, vol. 50, no. 5, pp. 741–747, 2009.

[21] T. W. Kim, D. H. Park, S. T. Lim, S.-J. Hwang, B.-K. Min, and J.-H. Choy, "Direct soft-chemical synthesis of chalcogen-doped manganese oxide 1D nanostructures: influence of chalcogen doping on electrode performance," *Small*, vol. 4, no. 4, pp. 507–514, 2008.

[22] S.-H. Park, Y.-S. Lee, and Y.-K. Sun, "Synthesis and electrochemical properties of sulfur doped-$Li_xMnO_{2-y}Sy$ materials for lithium secondary batteries," *Electrochemistry Communications*, vol. 5, no. 2, pp. 124–128, 2003.

[23] X. Chen and S. S. Mao, "Titanium dioxide nanomaterials: synthesis, properties, modifications and applications," *Chemical Reviews*, vol. 107, no. 7, pp. 2891–2959, 2007.

[24] H. Chi, Y. Li, Y. Xin, and H. Qin, "Boron-doped manganese dioxide for supercapacitor," *Chemical Communications*, vol. 50, pp. 13349–13352, 2014.

[25] E. K. Nyutu, C.-H. Chen, S. Sithambaram, V. M. B. Crisostomo, and S. L. Suib, "Systematic control of particle size in rapid

open-vessel microwave synthesis of K-OMS-2 nanofibers," *The Journal of Physical Chemistry C*, vol. 112, no. 17, pp. 6786–6793, 2008.

[26] D. Maniua, T. Iliescu, I. Ardelean, S. Cinta-Pinzaru, N. Tarcea, and W. Kiefer, "Raman study on B_2O_3-CaO glasses," *Journal of Molecular Structure*, vol. 651-653, pp. 485–488, 2003.

[27] K. Kumari, S. Ram, and R. K. Kotnala, "Self-controlled growth of Fe_3BO_6 crystallites in shape of nanorods from iron-borate glass of small templates," *Materials Chemistry and Physics*, vol. 129, no. 3, pp. 1020–1026, 2011.

[28] W.-H. Kuan and Y.-C. Chan, "pH-dependent mechanisms of methylene blue reacting with tunneled manganese oxide pyrolusite," *Journal of Hazardous Materials*, vol. 239-240, pp. 152–159, 2012.

[29] Y. X. Zhang, X. D. Hao, F. Li, Z. P. Diao, Z. Y. Guo, and J. Li, "pH-dependent degradation of methylene blue via rational-designed MnO 2 nanosheet-decorated diatomites," *Industrial & Engineering Chemistry Research*, vol. 53, no. 17, pp. 6966–6977, 2014.

[30] F. Polzer, S. Wunder, Y. Lu, and M. Ballauff, "Oxidation of an organic dye catalyzed by MnO_x nanoparticles," *Journal of Catalysis*, vol. 289, pp. 80–87, 2012.